

# Pulsar Polarization Arrays

Tao Liu,<sup>1,\*</sup> Xuzixiang Lou,<sup>1,†</sup> and Jing Ren<sup>2,‡</sup>

<sup>1</sup>*Department of Physics, The Hong Kong University of Science and Technology, Hong Kong S.A.R., P.R.China*

<sup>2</sup>*Institute of High Energy Physics, Chinese Academy of Sciences, Beijing 100049, P.R.China*

Pulsar timing arrays (PTAs) consisting of widely distributed and well-timed millisecond pulsars can serve as a galactic interferometer to measure gravitational waves. With the same data acquired for PTAs, we propose to develop pulsar polarization arrays (PPAs), to explore astrophysics and fundamental physics. As in the case of PTAs, PPAs are best suited to reveal temporal and spatial correlations at large scales that are hard to mimic by local noise. To demonstrate the physical potential of PPAs, we consider detection of ultralight axion-like dark matter (ALDM), through cosmic birefringence induced by its Chern-Simon coupling. Because of its tiny mass, the ultralight ALDM can be generated as a Bose-Einstein condensate, characterized by a strong wavy nature. Incorporating both temporal and spatial correlations of the signal, we show that PPAs have a potential to probe the Chern-Simon coupling up to  $\sim 10^{-14} - 10^{-17} \text{GeV}^{-1}$ , with a mass range  $\sim 10^{-27} - 10^{-21} \text{eV}$ .

## INTRODUCTION

Pulsars emit electromagnetic pulses with extraordinary regularity, with a period ranging from milliseconds to seconds. Although their emission mechanism has not been fully clarified, they play significant roles as astronomical clocks in testing the laws of fundamental physics.

Up to now about 3000 pulsars have been observed. Millisecond pulsars (MSPs) formed by mass and angular momentum transfer from a companion are especially stable. Pulsar timing arrays (PTAs) consisting of many well-timed MSPs thus have been applied as a galactic interferometer to measure nanohertz gravitational waves (GWs) [1, 2], complementing the ground-based and space-based detections. Recently, the explorations on the PTA targets were extended to dark matter (DM) physics such as periodic oscillations in gravitational potentials induced by ultralight axion-like DM (ALDM) [3–5], and Doppler or Shapiro effects induced by transiting objects associated with DM substructure [6–8].

The PTA programs take up a significant amount of resources of radio telescopes. Currently, over 80 MSPs are monitored by the global PTA network in the timespan of years. Future radio telescopes such as the Five-hundred meter Aperture Spherical Telescope (FAST) and the Square Kilometer Array (SKA) are expected to significantly increase the number of well-timed MSPs to the order of 1000 [9–11]. It is apparently of great value to fully explore the physical potential of telescope resources allocated to PTAs.

Pulsars are known to be typical astrophysical sources of linearly polarized light. As a by-product, the PTA programs usually measure the signal polarization profiles also. So we suggest to develop a pulsar polarization array (PPA), using the same data acquired for PTAs, to detect the temporal and spatial variations of the polarization angle (PA) of a signal. Currently, the polarization mea-

surements are used to infer Faraday rotation caused by the Galactic magnetic field [12–16], where no strong correlation between individual pulsars is expected. Nonetheless, as in the case of PTAs, PPAs are best suited to reveal temporal and spatial correlations at large scales that are hard to mimic by local noise.

In this letter, we demonstrate the potential reach of PPAs in testing fundamental physics by considering detection of ultralight ALDM. Ultralight ALDM behaves effectively as a classical scalar field in our galaxy. Its characteristic Chern-Simon interaction with photons leads to parity violation and induces cosmological birefringence [17–19]. Different from Faraday rotation, this ALDM-induced signal features an oscillatory signature, with the period being approximately the inverse of its mass (similar to the aforementioned oscillations in gravitational potentials [3–5]), and is insensitive to the light frequency. In last decades, polarization measurements for a variety of astrophysical light sources have been suggested to set constraints on this coupling [20–27]. However, spatial correlations of the signal among individual sources have not been properly considered. PPAs will then play an essential role in detecting the ALDM with its characteristic spatial correlations, as PTAs do for the stochastic gravitational wave backgrounds (SGWBs).

## ALDM-INDUCED COSMIC BIREFRINGENCE

An ensemble of ultralight ALDM particles forming a Bose-Einstein condensate is manifested as a classical scalar field ( $a$ ), with its Lagrangian given by

$$L \sim -\frac{1}{4}F_{\mu\nu}F^{\mu\nu} + \frac{1}{2}\partial^\mu a\partial_\mu a - \frac{1}{2}m_a^2 a^2 + \frac{g}{2}aF_{\mu\nu}\tilde{F}^{\mu\nu}, \quad (1)$$

where  $F^{\mu\nu}$ ,  $\tilde{F}^{\mu\nu}$  are electromagnetic field strength and its Hodge dual, and  $g$  is topological Chern-Simon coupling. While photons propagate in the ALDM field, this

topological interaction corrects the dispersion relations of their positive and negative circular polarization modes in a parity-violating manner, yielding

$$\omega_{\pm} \simeq k \pm g \left( \frac{\partial a}{\partial t} + \nabla a \cdot \frac{\mathbf{k}}{k} \right) \xrightarrow[\text{relativistic}]{\text{non-}} k \pm g \frac{\partial a}{\partial t}. \quad (2)$$

If these photons are linearly polarized, Eq. (2) implies a non-trivial rotation  $\Delta\theta$  to their PA, inducing the well-known effect of cosmological birefringence [17–19]. In the non-relativistic limit, the ALDM field is approximately given by [28]

$$a(\mathbf{x}, t) \approx \frac{\sqrt{\rho(\mathbf{x})}}{m_a} \int \alpha_{\mathbf{v}} \sqrt{f_{\mathbf{x}}(\mathbf{v})} \cos[\omega_a(t - \mathbf{v} \cdot \mathbf{x}) + \phi_{\mathbf{v}}] d^3\mathbf{v}. \quad (3)$$

Here the oscillating frequency  $\omega_a$  is approximately  $m_a$  in natural units; the random amplitude  $\alpha_{\mathbf{v}}$  and phase  $\phi_{\mathbf{v}}$  follow the Rayleigh and uniform distributions, respectively;  $\rho(\mathbf{x})$  denotes the ALDM density profile; and  $f_{\mathbf{x}}(\mathbf{v})$  is the velocity distribution at  $\mathbf{x}$ .

The PA rotation induced by ALDM can be probed by linearly polarized pulsar light [24, 25]. For detecting the pulsar signals, we consider average pulse profiles to overcome jitter noise due to the stochastic variation of individual ones [29, 30]. With a segment of observation over the timespan  $T_p$ , the data for the  $p$ -th MSP of the PPA consists of a time series of points  $\Delta\theta_{p,n} \equiv \Delta\theta_p(t_n)$  for  $n = 1, \dots, N_p$ , with each point being defined by one average profile over the folding time  $\tau_{\text{fold}}$ . To maintain the oscillation pattern of signals, we should keep  $m_a \tau_{\text{fold}} \lesssim 1$ . Then for the data point at  $t_n$ , the PA rotation is

$$\begin{aligned} \Delta\theta_{p,n} &= -g \int_{t_n - L_p}^{t_n} \frac{\partial}{\partial t} a(\mathbf{x}_p, t) dt \\ &= \frac{g}{m_a} \int \alpha_{\mathbf{v}} \left\{ \sqrt{\rho_p f_p(\mathbf{v})} \cos[m_a(t_n - L_p - \mathbf{v} \cdot \mathbf{x}_p) + \phi_{\mathbf{v}}] - \sqrt{\rho_e f_e(\mathbf{v})} \cos(m_a t_n + \phi_{\mathbf{v}}) \right\} d^3\mathbf{v}, \quad (4) \end{aligned}$$

where  $\rho_i \equiv \rho(\mathbf{x}_i)$ ,  $f_i(\mathbf{v}) \equiv f_{\mathbf{x}_i}(\mathbf{v})$ , with  $i = p, e$ , and we take  $\mathbf{x}_e = 0$ , with  $L_p = |\mathbf{x}_p|$  the distance from the pulsar to the Earth. Already for one pulsar, the ALDM-induced signal differs from Faraday rotation in three aspects. Firstly, the former features quasi-monochromatic oscillation around the frequency  $m_a$ , while no characteristic time dependence is expected for the latter. Secondly, the former has no radio frequency dependence, while the latter increases with the wavelength. Finally, the former relies only on the field profiles at two endpoints of photon traveling due to the topological nature of the parity-violating Chern-Simon coupling. As a result, Eq. (4) is characterized by a ‘‘pulsar’’ term and an ‘‘Earth’’ term.

For PPAs consisting of  $\mathcal{N} \gg 1$  pulsars, we can construct a signal vector

$$\mathbf{s} \equiv (\Delta\theta_{1,1}, \dots, \Delta\theta_{1,N_1}, \dots, \Delta\theta_{\mathcal{N},1}, \dots, \Delta\theta_{\mathcal{N},N_{\mathcal{N}}})^T, \quad (5)$$

for  $\Delta\theta_{p,n}$  in Eq. (4), with  $p = 1, \dots, \mathcal{N}$  and  $n = 1, \dots, N_p$ . Integrating out the random amplitude  $\alpha_{\mathbf{v}}$  and phase  $\phi_{\mathbf{v}}$ , the vector  $\mathbf{s}$  is found to follow a multivariable Gaussian distribution with zero mean, as in the case of Ref. [28]. The statistical properties are then determined by the covariance matrix  $\Sigma^{(s)}$ , with  $\Sigma_{p,n;q,m}^{(s)} = \langle \Delta\theta_{p,n} \Delta\theta_{q,m} \rangle$ . To simplify the phase space integral, we assume an isotropic distribution of  $\mathbf{v}$ . Given that this distribution peaks sharply at the characteristic velocity of cold DM in our galaxy, namely  $v_0 \sim 10^{-3}$  in natural units, we obtain

$$\begin{aligned} \Sigma_{p,n;q,m}^{(s)} &\approx \frac{g^2}{m_a^2} \left\{ \rho_e \cos(m_a \Delta t) \right. \\ &\quad + \sqrt{\rho_p \rho_q} \cos[m_a(\Delta t - \Delta L)] \frac{\sin y_{pq}}{y_{pq}} \\ &\quad - \sqrt{\rho_e \rho_p} \cos[m_a(\Delta t - L_p)] \frac{\sin y_{ep}}{y_{ep}} \\ &\quad \left. - \sqrt{\rho_e \rho_q} \cos[m_a(\Delta t + L_q)] \frac{\sin y_{eq}}{y_{eq}} \right\}, \quad (6) \end{aligned}$$

where  $\Delta t = t_{p,n} - t_{q,m}$ ,  $\Delta L \equiv L_p - L_q$ ,  $y_{pq} = \Delta x / l_c$  ( $\Delta x = |\mathbf{x}_p - \mathbf{x}_q|$ ),  $y_{ep(q)} = L_{p(q)} / l_c$ .  $l_c \equiv 1 / (m_a v_0)$  denotes the de Broglie coherence length for ALDM. For pulsar-related terms, the distance dependence in cosines is related to the light travel time between two objects. The sinc function ( $\sin y / y$ ) results from an average over different directions and measures the strength of spatial correlations. The spatial correlation degrades when the pulsar-pulsar and Earth-pulsar distances are far beyond the coherence length or  $y \gg 1$ .

It is instructive to compare the ALDM-induced signal in Eq. (6) with the response of PTAs to GWs. PTAs measure GW-induced changes of the light-travel time, which can be put as the Earth and pulsar terms as well. For isotropic SGWBs, the pulsar-related terms are suppressed in the large-antenna limit, i.e.  $\omega L_p \gg 1$ , with spatial correlations rapidly degrading. The sensitivity is then dominated by the Earth-Earth term, producing the quadrupolar spatial correlations among pulsars following the Hellings and Downs curve [31]. As a comparison, the Earth-Earth ( $\rho_e$ ) term in Eq. (6) features monopolar correlations, and cannot be distinguished from correlated noise universal for pulsars. Instead, the pulsar-related terms play a more decisive role for characterizing ALDM. Because of the  $l_c$  dependence of the sinc functions, spatial correlations degrade more slowly with distance than those do for SGWBs. The ALDM signal then can be greatly enhanced for pulsars near the galactic center, where the DM halo is denser. This is similar to the PTA detection of the ALDM-induced periodic oscillations in gravitational potentials [4]. Therefore, the detection of ultralight ALDM strongly motivates the incorporation of pulsars more broadly distributed in our galaxy for both PPAs and PTAs, in particular the ones near the galactic center.

## PULSAR CORRELATIONS

To see how pulsar auto- and cross-correlations improve the ALDM detectability, let us consider a simple case where the background is dominated by white noises  $\mathbf{n}$ . The hypothesized data  $\mathbf{d} = \mathbf{s} + \mathbf{n}$  then follows a multivariate Gaussian distribution with zero mean and a covariance matrix  $\Sigma = \Sigma^{(s)} + \Sigma^{(n)}$ , where the noise contribution is  $\Sigma_{p,n;q,m}^{(n)} = \lambda_p \delta_{p,q} \delta_{n,m}$ , with  $\lambda_p$  denoting the variance of noise for a given pulsar. The likelihood function for the data  $\mathbf{d}$  given the ALDM signal model is

$$\mathcal{L}(\theta|\mathbf{d}) = \frac{1}{\sqrt{\det[2\pi\Sigma]}} \exp\left[-\frac{1}{2}\mathbf{d}^T \cdot \Sigma^{-1} \cdot \mathbf{d}\right], \quad (7)$$

where  $\theta \equiv \{g, m_a, \theta^{\text{in}}\}$  is a vector of model parameters.  $\theta^{\text{in}} = (\theta_1^{\text{in}}, \dots, \theta_N^{\text{in}})$  denote intrinsic PAs of pulsars. Their values are usually unknown, so we will marginalize them by taking  $\mathcal{L}(g, m_a|\mathbf{d}) = \int \mathcal{L}(\theta|\mathbf{d}) \pi(\theta^{\text{in}}) d\theta^{\text{in}}$ , with a flat p.d.f.  $\pi(\theta^{\text{in}})$ . Then given a mass  $m_a$ , the exclusion limit for the coupling  $g$  is set by a test statistics [28]

$$q(g, m_a) \equiv 2[\ln \mathcal{L}(\hat{g}, m_a|\mathbf{d}) - \ln \mathcal{L}(g, m_a|\mathbf{d})], \quad (8)$$

where  $\hat{g}$  maximizes  $\mathcal{L}(g, m_a|\mathbf{d})$ . With  $q(g, m_a) = 0$  for  $g < \hat{g}$ , the upper limit at 95% C.L.  $g_{95\%}$  is given by  $q(g_{95\%}, m_a) = 2.71$ .

The projected sensitivities are estimated using Asimov form of the test statistics, by averaging over different noise realizations. Expanding the test statistics to the second order of  $\Sigma^{(s)}$  in the small-signal limit, we then obtain [32]

$$\langle q \rangle \approx \frac{1}{2} \sum_{p,q} \frac{1}{\lambda_p \lambda_q} \text{Tr} \left( \Sigma_{pq}^{(s)} \Sigma_{qp}^{(s)} \right), \quad (9)$$

where with a null-signal assumption we have  $\hat{g} = 0$ . The projected 95% C.L. upper limit of  $g$  is set by  $\langle q \rangle = 2.71$ .

Note that the test statistics considered above receives contributions from both auto-correlation of individual pulsars ( $\Sigma_{pp}^{(s)}$ ) and cross-correlation of different pulsars ( $\Sigma_{pq}^{(s)}$  with  $p \neq q$ ). The auto-correlation is significant when the noise variances are known well enough [33]. However, if backgrounds of unknown origins exist and share similar signatures of the signal, the cross-correlations become highly valuable. They can distinguish a signal with long-range spatial correlations, such as the one caused by ALDM, from the noises either non-correlated or correlated in different patterns. As a concrete example, let us consider the sinusoidal trends of pulsar PA rotation with a period of one to two years reported by NANOGrav [16]. As shown in Fig. 1, the auto-correlation of the data for PSRs J1918-0642 and J1909-3744 indicates anomalous peaks around the same period, which may be explained by ALDM physics with  $m_a \approx 7 \times 10^{-23}$  eV. But, by evaluating the cross-correlation of these two MSPs, we see null excess at this

$m_a$ . So the NANOGrav observations are unlikely to be related to ALDM. This demonstrates the essential role played by cross-correlations.

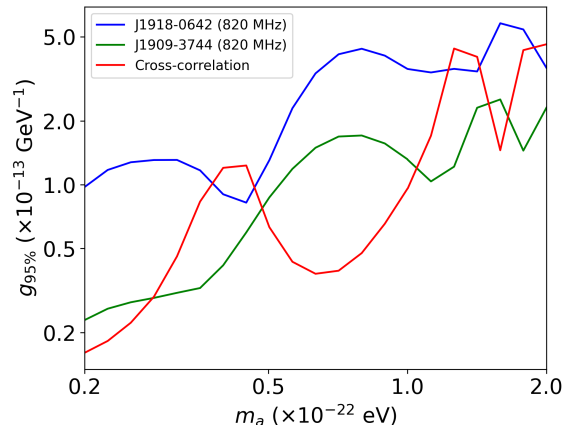


FIG. 1:  $g_{95\%}$  obtained from the NANOGrav data of J1918-0642 (820MHz) and J1909-3744 (820MHz) [16]. The blue and green lines are derived from pulsar auto-correlations, while the red line is based on their cross-correlation.

For the sake of completeness, we consider both auto- and cross-correlations of pulsars in the remainder of the paper, but in a comparative manner. Below let us get a picture on their roles in determining the PPA sensitivities through their contributions to  $\text{Tr}(\Sigma^{(s)}\Sigma^{(s)})$  in Eq. (9).

For the auto-correlation of a pulsar  $p$ , the matrix  $\Sigma_{pp}^{(s)}$  can be decomposed as

$$\Sigma_{pp}^{(s)} \approx A_{pp} \hat{\Sigma}_{pp}^{(s)}. \quad (10)$$

Here the matrix  $\hat{\Sigma}_{p,n;p,m}^{(s)} = \cos[m_a(t_{p,n} - t_{p,m})]$  encodes temporal correlations of data points, yielding  $\text{Tr}(\hat{\Sigma}_{pp}^{(s)} \hat{\Sigma}_{pp}^{(s)}) \propto N_p^2$  for the number of data points  $N_p$  sufficiently large. Complementary to  $\hat{\Sigma}_{pp}^{(s)}$ ,  $A_{pp} = (g^2/m_a^2)[\rho_e + \rho_p - 2\sqrt{\rho_e\rho_p} \cos(m_a L_p) \sin y_{ep}/y_{ep}]$  contains the messages on physical properties of axion, its halo profile and spatial distribution of pulsars. Relying on the pulsar location, the  $\rho_p$  term could be either dominant over or comparable to the  $\rho_e$  term in terms of their contributions to the trace. The last term of  $A_{pp}$  reflects the Earth-pulsar correlation, and is subject to a suppression when  $L_p \gg l_c$ . Approximately we have

$$\begin{aligned} & \text{Tr} \left( \Sigma_{pp}^{(s)} \Sigma_{pp}^{(s)} \right) \\ & \sim \frac{g^4}{m_a^4} N_p^2 \left[ \rho_e + \rho_p - 2\sqrt{\rho_e\rho_p} \cos(m_a L_p) \frac{\sin y_{ep}}{y_{ep}} \right]^2. \end{aligned} \quad (11)$$

Notably, the enhancement factor from temporal correlations, namely  $N_p^2$ , is not very sensitive to the distribution of sampled points and hence the data-taking strategy.

For cross-correlation of two pulsars  $p$  and  $q$ , the matrix  $\Sigma_{pq}^{(s)}$  can be decomposed as

$$\Sigma_{pq}^{(s)} \approx A_{pq} \hat{\Sigma}_{pq}^{(s)} + A'_{pq} \hat{\Sigma}'_{pq}{}^{(s)}. \quad (12)$$

Now the temporal correlations are encoded in  $\hat{\Sigma}_{p,n;q,m}^{(s)} = \cos[m_a(t_{p,n} - t_{q,m})]$  and  $\hat{\Sigma}'_{p,n;q,m} = \sin[m_a(t_{p,n} - t_{q,m})]$ , while the spatial correlations are manifested by their coefficients. Approximately, we have

$$\begin{aligned} \text{Tr} \left( \mathbf{\Sigma}_{pq}^{(s)} \mathbf{\Sigma}_{pq}^{(s)} \right) &\sim \frac{g^4}{m_a^4} N_p N_q \left[ \rho_e^2 + \rho_p \rho_q \frac{\sin^2 y_{pq}}{y_{pq}^2} \right. \\ &\left. + 2\rho_e \sqrt{\rho_p \rho_q} \cos(m_a \Delta L) \frac{\sin y_{pq}}{y_{pq}} + f(y_{ep}, y_{eq}) \right]. \end{aligned} \quad (13)$$

As in the case of auto-correlations, an enhancement factor ( $\sim N_p N_q$ ) appears due to temporal correlations regardless of the distribution of sampled points. For spatial correlation, the universal cross-correlation of the Earth terms ( $\sim \rho_e^2$ ) always contributes. But, the most interesting contribution is from the  $\rho_p \rho_q$  term which exclusively encodes the cross-correlation of physics around two pulsars, *e.g.*  $\rho_p$  and  $\rho_q$ , and hence distinguishes itself from others by nature. As one of the core observables of PPAs, this term can greatly enhance the detection efficiency especially for pulsars around the galactic center and with the separation not considerably bigger than the axion coherence length, namely  $\Delta x/l_c < \sqrt{\rho_p \rho_q}/\rho_e$ .

As it happens to the GW detections with PTAs, the uncertainty of pulsar distance may significantly impact the sensitivity of PPAs. In the former case, this uncertainty makes the phase of pulsar-related terms unpredictable, and the current sensitivities are dominated by the Earth term [34, 35]. For PPAs, this uncertainty can easily cause a rapid oscillation of the Earth-pulsar terms in Eqs. (11) and (13) and hence eliminates their contributions. However, there is no such oscillation for the  $\rho_p \rho_q$  term in Eq. (13), for which the distance uncertainty enters only through the sinc function. Below we will marginalize the distance uncertainty for evaluating  $\langle q \rangle$ . Currently, the pulsar distance is inferred mostly from the observed dispersion measure, where the uncertainty may reach a level  $\sim 100\%$ . Model-independent measurements (e.g. VLBI astrometry) can push the distance error down to  $\sim 20\%$ , but only for dozens of MSPs [36]. The situation may be greatly improved in the upcoming FAST/SKA era [37]. By using timing parallax methods, a precision  $\sim 20\%$  could be achieved, even for MSPs around the galactic center [38].

## PROJECTED SENSITIVITIES OF PPAS

Below we will demonstrate the projected sensitivity of PPAs to detect ultralight ALDM. As counterparts of PTAs at different stages, three PPA scenarios will be considered, including

- Near PPA (NPPA): 100 MSPs distributed around the Earth, which we take as the observed MSPs in the ATNF Pulsar Catalogue [39] with  $0.50 \text{ kpc} \leq L_p \leq 1.52 \text{ kpc}$ . Each pulsar has  $N_p = 100$  data

points with a constant time separation over  $T_p = 10$  years. The noise variance is assumed to be  $\lambda_p = (1 \text{ deg})^2$ , typical for the current PA measurements from PTAs [15].

- Far PPA (FPPA): 100 MSPs randomly but uniformly distributed within a  $(1.0 \text{ kpc})^3$  cube around galactic center, *i.e.*, the bulge area.  $N_p$ ,  $T_p$  and  $\lambda_p$  for each pulsar are assumed the same as above.
- Optimal PPA (OPPA): 1000 MSPs randomly distributed, which we take following a distribution fitting the MSP data in the ATNF Pulsar Catalogue [39]. As a more aggressive choice of parameters for each pulsar, we assume  $T_p = 30$  year, with an observational cadence of 1/(one week) and hence  $N_p \approx 1500$  data points.  $\lambda_p$  is the same as above.

Note that these scenarios may not be fully realistic, but their performances can serve as inputs for optimizing later PTA+PPA operations.

Another input is the galactic density profile of ultralight ALDM. It is known that ALDM can form a cored soliton-like structure in its halo due to quantum pressure, at a distance from the center  $r \lesssim l_c$  [40]. But, a full simulation for the overall profile of halo with various  $m_a$  values and relic-abundance shares in DM remains absent in literatures. So we simply model this halo with a soliton+NFW profile [41], namely

$$\rho(r) = \kappa \times \begin{cases} \frac{0.019 \left(\frac{m_a}{m_{a,0}}\right)^{-2} \left(\frac{r_c}{1 \text{ kpc}}\right)^{-4}}{[1 + 9.1 \times 10^{-2} \left(\frac{r}{r_c}\right)^2]^8} M_\odot \text{pc}^{-3}, & \text{for } r < l_c. \\ \frac{\rho_0}{r/R_H(1+r/R_H)^2}, & \text{for } r > l_c. \end{cases} \quad (14)$$

which is smoothened with hyperbolic tangent function at  $r \sim l_c$ . Here  $r_c \approx 100 \text{ pc} \times m_{a,0}/m_a$  is obtained by fitting to the observed DM density at galactic center [40], with  $m_{a,0} = 10^{-22} \text{ eV}$ .  $\rho_0 \approx 0.014 M_\odot \text{pc}^{-3}$  and  $R_H = 16.1 \text{ kpc}$  are NFW parameters normalized with the local DM density near the Earth [42].  $\kappa = \Omega_a/\Omega_{\text{DM}}$  represents the relic abundance of ALDM, which is considerably constrained by the CMB anisotropies for  $m_a \lesssim 10^{-24} \text{ eV}$  [43].

The projected  $g_{95\%}$  limits as a function of  $m_a$  are displayed in Fig. 2. For each of the three PPA scenarios, we present the constraints from auto- and cross-correlation separately, in order to highlight their respective roles in detection.<sup>1</sup> A general picture is the following. The projected  $g_{95\%}$  values evolve with three different stages as  $m_a$  decreases: decrease first, then stay approximately flat,

<sup>1</sup> Note that we impose constraints on ALDM for a wide range of  $m_a$  through its overall contribution. For detection, properly estimating the oscillation frequency when  $m_a \ll 1/T_p$  or  $m_a \gg N_p/T_p$  is non-trivial.

and finally increase. The cross-correlation limits are typically stronger than the auto-correlation ones, except in the large  $m_a$  region for FPPA.

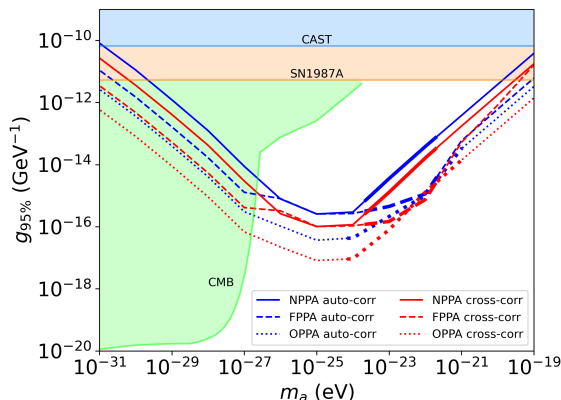


FIG. 2: Projected  $g_{95\%}$  with NPPA, FPPA and OPPA, based on auto- and cross-correlations of pulsars. Segments of the curves are thickened to highlight the region of  $1/T_p < m_a < N_p/T_p$ , where  $m_a$  can be inferred from discrete Fourier analysis. The blue and orange regions are excluded by the CAST [44] and SN1987A measurements [45] that are insensitive to the  $m_a$  values. The green is excluded by the CMB measurements of isotropic cosmological birefringence [46, 47], which is significant for  $m_a \lesssim 10^{-27}$  eV where ALPs behave more like dark energy.

Consider NPPA first for details. For  $m_a \gtrsim 10^{-24}$  eV, NPPA locates in the NFW halo and hence  $\rho_p \sim \rho_e$  independent of  $m_a$ . The  $g_{95\%}$  value is essentially determined by the  $(\rho_e + \rho_p)^2$  terms in Eq. (11) and the Earth ( $\rho_e^2$ ) term in Eq. (13). So we approximately have  $g_{95\%} \sim m_a \lambda^{1/2} N_p^{-1/2} \rho_e^{-1/2} \mathcal{N}^{-1/4}$  for auto-correlation and one enhanced by  $\mathcal{N}^{-1/4}$  for cross-correlation. The ALDM around the Earth can induce similar oscillations in CMB polarization also. But the constraint is weaker [48]. For  $10^{-26} \lesssim m_a \lesssim 10^{-24}$  eV, the ALDM soliton encompasses NPPA, and the  $m_a$  dependence in  $g^4/m_a^4$  is cancelled by that in the soliton profile. So  $g_{95\%}$  is approximately flat except a small decrease at  $m_a \sim 10^{-25}$  eV due to the CMB constraints on  $\kappa$  [43]. As  $m_a$  falls below  $10^{-26}$  eV, the Earth-pulsar terms yield a large cancellation. The  $g_{95\%}$  limits get weakened as  $\propto m_a^{-1}$ . Compared to NPPA, FPPA benefits from soliton-enhanced  $\rho_p$ . The limit is significantly improved for  $m_a \sim 10^{-22}$  eV due to a large contrast of DM density  $\rho_p/\rho_e \sim 10^5$ . Above  $m_a \sim 10^{-21}$  eV, the cross-correlation limit degrades with decreasing coherence length  $l_c$  and approaches that of NPPA. OPPA benefits from the increased  $\mathcal{N}$  and  $N_p$ . The enhancement from  $\mathcal{N}$  is most significant for intermediate  $m_a$  when most MSPs are spatially well-correlated. Given  $g_{95\%} \propto \lambda^{1/2}$ , the limits could be one order stronger if  $\lambda \sim (0.1\text{deg})^2$  can be reached in the future. Apparently, the projected PPA limits form a great complementarity with the existing bounds.

## SUMMARY AND OUTLOOK

In this letter we propose the development of PPAs with the same data acquired for PTAs, and demonstrate their physical potential using the detection of ultralight ALDM as an example. Two important directions for future explorations can be immediately seen. Firstly, we can cross-correlate PPAs and PTAs to further strengthen the ALDM detectability, given that the periodic oscillations in PA rotation have the same origin as the oscillations in gravitational potentials [3–5]. Secondly, PPAs provide a new tool for exploring fundamental physics. To fully resolve the physics targets such as new parity-violating origins of cosmic birefringence, it is valuable to synergize PPAs with other experimental/observational tools to improve the capability to distinguish different scenarios. We leave these explorations to a later work.

## Acknowledgments

We would greatly thank J. M. Cordes for highly valuable discussions on PTAs and pulsar polarization measurements, and constructive comments on this manuscript. T. Liu is supported by the Collaborative Research Fund under Grant No. C6017-20G which is issued by Research Grants Council of Hong Kong S.A.R. J. Ren is supported by the Institute of High Energy Physics, Chinese Academy of Sciences, under Contract No. Y9291220K2.

## A. Noise for PA Measurements

The measured PA for pulsar light can be manifested as [13],

$$\begin{aligned} \text{PA} = & \text{PA}_{\text{ALDM}} + \text{PA}_{\text{source}} + \text{PA}_{\text{FR}} \\ & + \text{PA}_{\text{instr}} + \text{PA}_{\text{noise}} + \text{PA}_{\text{jitter}}. \end{aligned} \quad (15)$$

Here  $\text{PA}_{\text{ALDM}}$  represents the signal of ALDM.  $\text{PA}_{\text{source}}$  denotes variations due to changes in orientation of the pulsar or its magnetosphere.  $\text{PA}_{\text{FR}}$  quantifies Faraday rotation in the interstellar medium and Earth's ionosphere.  $\text{PA}_{\text{instr}}$  is related to a conversion of absolute PA on the sky to that measured in the instrumental frame by referring to a calibrator pulsar (or other bright polarized sources).  $\text{PA}_{\text{noise}}$  denotes the radiometer noise that is inversely proportional to the signal-to-noise ratio (SNR).  $\text{PA}_{\text{jitter}}$  is from jitter noise unique to pulsars. It is related to a stochastic variation of single pulse amplitude and phase due to activities in the magnetosphere of neutron stars [13, 29, 30], and is independent of the SNR. The jitter effects can be reduced by considering average polarization profile, namely the average of a sufficiently large number of pulses. The variance of jitter

noise  $\lambda$  is inversely proportional to the number of averaged pulses  $N_{\text{ave}}$ . A rough estimation indicates that  $\lambda \sim 0.7/N_{\text{ave}}$  [13].

Among the latter two types of noise, the radiometer noise dominates for fainter pulsars with a small SNR, while the jitter noise limits the sensitivity of bright pulsars. For example, the calibrator pulsar B0540+23 has radiometer noise  $\sim 0.1$  deg and jitter noise  $\sim 1$  deg, with a pulsing period  $P_0 \sim \mathcal{O}(0.1)$  s and the folding time  $\tau_{\text{fold}} \sim 2$  mins [13]. For MSP J0437–4715 monitored by PPTA, the jitter noise is  $\sim 0.1$  deg with  $P_0 \sim \mathcal{O}(1)$  ms and  $\tau_{\text{fold}} \sim 1$  hr, while the reported error is  $\sim 1$  deg [15], indicating an error budget dominated by the radiometer noise. In the FAST/SKA era, the jitter noise is expected to dominate for the majority of bright MSPs [13].

If jitter noise dominates the error budget of PPA measurements, the sensitivity can be strongly constrained by the available telescope resources. Given a fixed total telescope time  $T_{\text{total}}$  for a PPA program, there is a trade-off between the number of averaged pulses  $N_{\text{ave}}$ , the number of pulsars in the array  $\mathcal{N}$ , and the number of data points  $N_p$ , which is manifested as  $\sum_{p=1}^{\mathcal{N}} \tau_{\text{fold}} N_p = T_{\text{total}}$ , with  $\tau_{\text{fold}} = P_0 N_{\text{ave}}$ . If  $N_p$  and  $P_0$  are universal for all pulsars in the array, the constraint becomes  $P_0 N_{\text{ave}} N_p \mathcal{N} = T_{\text{total}}$  or  $N_p \mathcal{N} / \lambda \sim T_{\text{total}} / P_0$ . The average test statistics in (9) is then  $\langle q \rangle \propto N_p^2 (\sum_{p,q} A_{pq}^2) / \lambda^2$ . If all pulsars are cross-correlated,  $\langle q \rangle \propto (N_p \mathcal{N} / \lambda)^2 \propto (T_{\text{total}} / P_0)^2$  is fixed by  $T_{\text{total}}$  regardless of the choice of  $N_{\text{ave}}$  and  $\mathcal{N}$ . As for auto-correlation, we have  $\langle q \rangle \propto N_p^2 \mathcal{N} / \lambda^2 \propto (T_{\text{total}} / P_0)^2 / \mathcal{N}$ . Having a larger array thus may not be favored, given the limited resources.

However, as we highlight in the main text, cross-correlations play an essential role in distinguishing a signal with long-range spatial correlations from the non-correlated noise and in identifying its origin with the specific pattern of spatial correlations. Thus, forming arrays with the telescope resources more evenly distributed for a broad range of pulsars in our galaxy can maximize the potential physical reach for both PPAs and PTAs.

## B. More on Pulsar Correlations

For auto-correlation of pulsars, temporal correlation is encoded in the matrix  $\hat{\Sigma}_{pp}^{(s)}$ . In an ideal case where data points of each pulsar ( $N_p$ ) are sampled with a constant separation ( $\tau_p$ ) for the observation duration  $T_p = N_p \tau_p$ , its contribution to the average test statics  $\langle q \rangle$  is

$$\text{Tr} \left( \hat{\Sigma}_{pp}^{(s)} \hat{\Sigma}_{pp}^{(s)} \right) = \frac{1}{2} \left[ N_p^2 + \left( \frac{\sin(m_a T_p)}{\sin(m_a \tau_p)} \right)^2 \right]. \quad (16)$$

For  $m_a \ll 1/T_p$ , we have simply  $\text{Tr} \left( \hat{\Sigma}_{pp}^{(s)} \hat{\Sigma}_{pp}^{(s)} \right) \sim N_p^2$ . When  $1/T_p \ll m_a \ll 1/\tau_p$ , the second term becomes  $N_p^2 (\sin y / y)^2$  with  $y = m_a T_p$ , and is much smaller than

the first one for  $y \gg 1$ . If  $1/\tau_p \ll m_a \ll 1/\tau_{\text{fold}}$ , here  $\tau_{\text{fold}}$  is folding time of each data point,  $\sin(m_a T_p) / \sin(m_a \tau_p)$  oscillates between  $N_p$  and  $-N_p$ , and the trace reaches the maximum when  $m_a \tau_p$  is an integer multiple of  $\pi$ . Hence, this trace ranges from  $N_p^2/2$  to  $N_p^2$ .

In reality, data points are often taken far from uniformly. To see the impact, we sample  $t_{p,n} \in [0, T_p]$  randomly for  $m_a T_p \gg 1$ . We find that  $\text{Tr}(\hat{\Sigma}_{pp}^{(s)} \hat{\Sigma}_{pp}^{(s)})$  is bounded from below by  $N_p^2/2$ , and the deviation from that becomes smaller as  $N_p$  and  $m_a T_p$  increase. Numerically, this is manifested as

$$\frac{\text{Tr}(\hat{\Sigma}_{pp}^{(s)} \hat{\Sigma}_{pp}^{(s)})}{(N_p^2/2)} - 1 \propto \frac{1}{N_p} \frac{1}{m_a T_p}. \quad (17)$$

Thus, for sufficiently large  $N_p$ , the trace is approximately

$$\begin{aligned} \text{Tr} \left( \hat{\Sigma}_{pp}^{(s)} \hat{\Sigma}_{pp}^{(s)} \right) &\sim A_{pp}^2 N_p^2 \\ &\approx \frac{g^4}{m_a^4} N_p^2 \left[ \rho_e + \rho_p - 2\sqrt{\rho_e \rho_p} \cos(m_a L_p) \frac{\sin y_{ep}}{y_{ep}} \right]^2. \end{aligned} \quad (18)$$

The temporal correlation leads to an  $N_p^2$  enhancement regardless of the distribution of the sampled points.

For cross-correlation, the coefficients for the two matrices  $\hat{\Sigma}_{pq}^{(s)}$  and  $\hat{\Sigma}'_{pq}^{(s)}$  in Eq. (12) are

$$\begin{aligned} A_{pq} &= \frac{g^2}{m_a^2} \left[ \rho_e + \sqrt{\rho_p \rho_q} \cos(m_a \Delta L) \frac{\sin y_{pq}}{y_{pq}} - \sqrt{\rho_e \rho_p} \right. \\ &\quad \left. \cos(m_a L_p) \frac{\sin y_{ep}}{y_{ep}} - \sqrt{\rho_e \rho_q} \cos(m_a L_q) \frac{\sin y_{eq}}{y_{eq}} \right] \\ A'_{pq} &= \frac{g^2}{m_a^2} \left[ \sqrt{\rho_p \rho_q} \sin(m_a \Delta L) \frac{\sin y_{pq}}{y_{pq}} - \sqrt{\rho_e \rho_p} \sin(m_a L_p) \right. \\ &\quad \left. \frac{\sin y_{ep}}{y_{ep}} + \sqrt{\rho_e \rho_q} \sin(m_a L_q) \frac{\sin y_{eq}}{y_{eq}} \right], \end{aligned} \quad (19)$$

where  $A_{pq}$  contains an Earth-Earth term, while  $A'_{pq}$  involves the pulsar-related terms only.

For temporal correlation, again we consider an ideal case with a uniform sampling first. Assuming that the time series for pulsar  $p$  and  $q$  contain  $N_p$  and  $N_q$  data points with time separation  $\tau_p$  and  $\tau_q$ , we find

$$\begin{aligned} \text{Tr} \left( \hat{\Sigma}_{pq}^{(s)} \hat{\Sigma}_{pq}^{(s)} \right) &= \frac{1}{2} \left[ N_p N_q + \frac{\sin(m_a T_p)}{\sin(m_a \tau_p)} \frac{\sin(m_a T_q)}{\sin(m_a \tau_q)} \cos \Theta \right] \\ \text{Tr} \left( \hat{\Sigma}'_{pq}^{(s)} \hat{\Sigma}'_{pq}^{(s)} \right) &= \frac{1}{2} \left[ N_p N_q - \frac{\sin(m_a T_p)}{\sin(m_a \tau_p)} \frac{\sin(m_a T_q)}{\sin(m_a \tau_q)} \cos \Theta \right] \\ \text{Tr} \left( \hat{\Sigma}_{pq}^{(s)} \hat{\Sigma}'_{pq}^{(s)} \right) &= \frac{1}{2} \frac{\sin(m_a T_p)}{\sin(m_a \tau_p)} \frac{\sin(m_a T_q)}{\sin(m_a \tau_q)} \sin \Theta, \end{aligned} \quad (20)$$

where  $\Theta = m_a (t_{p,N_p} - t_{q,N_q} + t_{p,1} - t_{q,1})$  quantifies the time difference of the initial and final data points for the two pulsars. The trace of the signal covariance matrix

square is

$$\begin{aligned} \text{Tr} \left( \hat{\Sigma}_{pq}^{(s)} \hat{\Sigma}_{pq}^{(s)} \right) &= \frac{1}{2} (A_{pq}^2 + A_{pq}'^2) N_p N_q \\ &+ \frac{1}{2} (A_{pq}^2 - A_{pq}'^2) \frac{\sin(m_a T_p)}{\sin(m_a \tau_p)} \frac{\sin(m_a T_q)}{\sin(m_a \tau_q)} \cos \Theta \\ &+ A_{pq} A_{pq}' \frac{\sin(m_a T_p)}{\sin(m_a \tau_p)} \frac{\sin(m_a T_q)}{\sin(m_a \tau_q)} \sin \Theta. \end{aligned} \quad (21)$$

Different from the first term, which tends to be dominant, the other two terms could be important only when  $m_a \tau_{p,q}$  are both around an integer multiple of  $\pi$ .

The influence of non-uniformness of data points for the cross-correlation is more involved. With random samplings, we find that  $\text{Tr}(\hat{\Sigma}_{pq}^{(s)} \hat{\Sigma}_{pq}^{(s)}) - N_p N_q / 2$ ,  $\text{Tr}(\hat{\Sigma}_{pq}^{(s)} \hat{\Sigma}_{pq}'^{(s)}) - N_p N_q / 2$  and  $\text{Tr}(\hat{\Sigma}_{pq}'^{(s)} \hat{\Sigma}_{pq}'^{(s)})$  all follow a narrow distribution around zero, and the deviations get smaller as  $N_p N_q$  and  $m_a T_j$  increase. Therefore, for sufficiently large  $N_{p,q}$ , a good approximation of cross-correlation is given by (13), up to some terms suppressed if  $y_{ep,eq} \gg 1$ . The dominant  $(A_{pq}^2 + A_{pq}'^2)$  term in Eq. (21) eventually leads to the pulsar-pulsar term in Eq. (13) which is free of any oscillations caused by light traveling from pulsars to the Earth.

---

\* Electronic address: taoliu@ust.hk

† Electronic address: xlouaa@connect.ust.hk

‡ Electronic address: renjing@ihep.ac.cn

- [1] A. N. Lommen, Rept. Prog. Phys. **78**, 124901 (2015).
- [2] C. Tiburzi, Publ. Astron. Soc. Austral. **35**, e013 (2018), 1802.05076.
- [3] A. Khmel'nitsky and V. Rubakov, JCAP **02**, 019 (2014), 1309.5888.
- [4] I. De Martino, T. Broadhurst, S. H. Henry Tye, T. Chiueh, H.-Y. Schive, and R. Lazkoz, Phys. Rev. Lett. **119**, 221103 (2017), 1705.04367.
- [5] N. K. Porayko et al., Phys. Rev. D **98**, 102002 (2018), 1810.03227.
- [6] J. A. Dror, H. Ramani, T. Trickle, and K. M. Zurek, Phys. Rev. D **100**, 023003 (2019), 1901.04490.
- [7] H. Ramani, T. Trickle, and K. M. Zurek, JCAP **12**, 033 (2020), 2005.03030.
- [8] V. S. H. Lee, S. R. Taylor, T. Trickle, and K. M. Zurek (2021), 2104.05717.
- [9] R. Smits, M. Kramer, B. Stappers, D. R. Lorimer, J. Cordes, and A. Faulkner, Astron. Astrophys. **493**, 1161 (2009), 0811.0211.
- [10] G. Hobbs, S. Dai, R. N. Manchester, R. M. Shannon, M. Kerr, K. J. Lee, and R. Xu, Res. Astron. Astrophys. **19**, 020 (2019), 1407.0435.
- [11] G. Janssen et al., PoS **AASKA14**, 037 (2015), 1501.00127.
- [12] R. Beck (2009), 0912.2918.
- [13] J. M. Weisberg, J. E. Everett, J. M. Cordes, J. J. Morgan, and D. G. Brisbin, The Astrophysical Journal **721**, 1044 (2010).
- [14] W. Yan et al., Mon. Not. Roy. Astron. Soc. **414**, 2087 (2011), 1102.2274.
- [15] W. Yan et al., Astrophys. Space Sci. **335**, 485 (2011), 1105.4213.
- [16] H. M. Wahl et al. (NANOGrav) (2021), 2104.05723.
- [17] S. M. Carroll, G. B. Field, and R. Jackiw, Physical Review D **41**, 1231 (1990).
- [18] S. M. Carroll and G. B. Field, Physical Review D **43**, 3789 (1991).
- [19] D. Harari and P. Sikivie, Physics Letters B **289**, 67 (1992).
- [20] S. M. Carroll, G. B. Field, and R. Jackiw, Phys. Rev. D **41**, 1231 (1990).
- [21] R. Antonucci, Ann. Rev. Astron. Astrophys. **31**, 473 (1993).
- [22] M. M. Ivanov, Y. Y. Kovalev, M. L. Lister, A. G. Panin, A. B. Pushkarev, T. Savolainen, and S. V. Troitsky, JCAP **02**, 059 (2019), 1811.10997.
- [23] T. Fujita, R. Tazaki, and K. Toma, Phys. Rev. Lett. **122**, 191101 (2019), 1811.03525.
- [24] T. Liu, G. Smoot, and Y. Zhao, Phys. Rev. D **101**, 063012 (2020), 1901.10981.
- [25] A. Caputo, L. Sberna, M. Frias, D. Blas, P. Pani, L. Shao, and W. Yan, Physical Review D **100**, 063515 (2019).
- [26] S. Chigusa, T. Moroi, and K. Nakayama, Phys. Lett. B **803**, 135288 (2020), 1911.09850.
- [27] Y. Chen, J. Shu, X. Xue, Q. Yuan, and Y. Zhao, Phys. Rev. Lett. **124**, 061102 (2020), 1905.02213.
- [28] J. W. Foster, N. L. Rodd, and B. R. Safdi, Physical Review D **97**, 123006 (2018).
- [29] J. M. Cordes and G. S. Downs, Astrophysical Journal Supplement Series **59**, 343 (1985).
- [30] J. M. Cordes, A. Wolszczan, R. J. Dewey, M. Blaskiewicz, and D. R. Stinebring, Astrophys. J. **349**, 245 (1990).
- [31] R. W. Hellings and G. S. Downs, Astrophys. J., Lett. Ed.; (United States) **265**, L39 (1983).
- [32] J. W. Foster, Y. Kahn, R. Nguyen, N. L. Rodd, and B. R. Safdi, arXiv preprint arXiv:2009.14201 (2020).
- [33] J. D. Romano and N. J. Cornish, Living Rev. Rel. **20**, 2 (2017), 1608.06889.
- [34] Y. Wang, S. D. Mohanty, and F. A. Jenet, Astrophys. J. **795**, 96 (2014), 1406.5496.
- [35] X. Zhu, L. Wen, J. Xiong, Y. Xu, Y. Wang, S. D. Mohanty, G. Hobbs, and R. N. Manchester, Mon. Not. Roy. Astron. Soc. **461**, 1317 (2016), 1606.04539.
- [36] A. T. Deller et al., Astrophys. J. **875**, 100 (2019), 1808.09046.
- [37] A. Lyne and F. Graham-Smith, *Pulsar astronomy*, 48 (Cambridge University Press, 2012).
- [38] R. Smits, S. J. Tingay, N. Wex, M. Kramer, and B. Stappers, Astronomy & Astrophysics **528**, A108 (2011), 1101.5971.
- [39] R. N. Manchester, G. B. Hobbs, A. Teoh, and M. Hobbs, The Astronomical Journal **129**, 1993 (2005), astro-ph/0412641.
- [40] H.-Y. Schive, T. Chiueh, and T. Broadhurst, Nature Phys. **10**, 496 (2014), 1406.6586.
- [41] D. J. E. Marsh, Phys. Rept. **643**, 1 (2016), 1510.07633.
- [42] F. Nesti and P. Salucci, **2013**, 016 (2013), URL <https://doi.org/10.1088/1475-7516/2013/07/016>.
- [43] R. Hložek, D. J. E. Marsh, and D. Grin, Monthly Notices of the Royal Astronomical Society **476**, 3063–3085 (2018), ISSN 1365-2966, URL <http://dx.doi.org/10.1093/mnras/sty271>.
- [44] V. Anastassopoulos, S. Aune, K. Barth, A. Belov, H. Bräuninger, G. Cantatore, J. M. Carmona, J. F. Cas-

- tel, S. A. Cetin, F. Christensen, et al., *Nature Physics* **13**, 584 (2017), URL <https://doi.org/10.1038/nphys4109>.
- [45] A. Payez, C. Evoli, T. Fischer, M. Giannotti, A. Mirizzi, and A. Ringwald, *Journal of Cosmology and Astroparticle Physics* **2015**, 006–006 (2015), ISSN 1475-7516, URL <http://dx.doi.org/10.1088/1475-7516/2015/02/006>.
- [46] N. Aghanim, M. Ashdown, J. Aumont, C. Baccigalupi, M. Ballardini, A. J. Banday, R. B. Barreiro, N. Bartolo, S. Basak, and et al., *Astronomy & Astrophysics* **596**, A110 (2016), ISSN 1432-0746, URL <http://dx.doi.org/10.1051/0004-6361/201629018>.
- [47] T. Fujita, K. Murai, H. Nakatsuka, and S. Tsujikawa, *Physical Review D* **103** (2021), ISSN 2470-0029, URL <http://dx.doi.org/10.1103/PhysRevD.103.043509>.
- [48] M. A. Fedderke, P. W. Graham, and S. Rajendran, *Phys. Rev. D* **100**, 015040 (2019), 1903.02666.